

Isogeometric Analysis on Triangulations

Noah Jaxon (njaxon@hawk.iit.edu) Xiaoping Qian (qian@iit.edu)

*Department of Mechanical, Materials and Aerospace Engineering
Illinois Institute of Technology, Chicago, IL 60616, USA*

Abstract

We present a method for isogeometric analysis on triangulation of a domain bounded by NURBS curves. In this method, both the geometry and the physical field are represented by bivariate splines in Bernstein Bézier form over the triangulation. We describe a set of procedures to construct a parametric domain and its triangulation from a given physical domain, construct C^r -smooth basis functions over the domain, and establish a rational Triangular Bézier Spline (rTBS) based geometric mapping that C^r -smoothly maps the parametric domain to the physical domain and exactly recovers the NURBS boundaries at the domain boundary. As a result, this approach can achieve automated meshing of objects with complex topologies and allow highly localized refinement. Isogeometric analysis of problems from linear elasticity and advection-diffusion analysis is demonstrated.

Key words: Isogeometric analysis, rational triangular Bézier, bivariate splines, NURBS, Bernstein-Bézier form

1. Introduction

Isogeometric analysis is a technique of numerical analysis that uses basis functions commonly found in CAD geometries to represent both geometry and physical fields in the solution of problems governed by partial differential equations (PDE) [1][2]. Non-uniform rational B-splines (NURBS) are the *de facto* standard for geometric representation in CAD systems. The use of a NURBS-compatible basis in the solution of physical problems therefore leads to the elimination of geometric-approximation error in even the coarsest mesh. The increased continuity of the NURBS basis has led to significant numerical advantages over traditional Lagrange polynomials and other C^0 inter-element continuity based finite element analysis, e.g. improved convergence rate on a per degree-of-freedom (DOF) basis [2]. However, NURBS-based isogeometric analysis also faces challenges. For example, it is challenging to automatically construct NURBS-based volumetric representation of a complex physical domain since CAD geometries only contain boundary representation of the domain; Further, the tensor-product structure of NURBS makes it harder to perform local mesh refinement as is commonly desired during analysis.

Recently, significant progress has been made in addressing these challenges. For example, the swept volume [3], harmonic functions [4], multi-block [5], and Coons patch [6] techniques have recently been developed to construct

NURBS representations of volumetric domains. To extend NURBS representation to complex topologies while also allowing for adaptive refinement, T-splines [7] have been used in isogeometric analysis [8][9][10]. Methods for constructing T-spline based parametrization of the domain are being developed [11][12]. Among alternate isogeometric representation and analysis techniques under development, a technique based on subdivision solids has recently been proposed [13]. Further, boundary-integral based isogeometric analysis techniques [14][15] seek to effectively bypass the need for volumetric parametrization.

We present an alternative approach to isogeometric analysis with the goal of achieving automatic discretization of the physical domain while eliminating geometric approximation error, allowing local refinement of the discretization and making it applicable to complex topologies. Our approach is based on triangulations of physical domains where both the geometry and physical field are represented by C^r -continuous multivariate splines in their Bernstein-Bézier form. In this paper, we restrict our attention to two-dimensional problems and bivariate splines. In our method, we first construct a polygonal parametric domain $\hat{\Omega}$ that mimics the NURBS-bounded physical domain Ω . We then obtain a triangulation T of $\hat{\Omega}$, on which a Bernstein-Bézier form of a C^r bivariate spline basis is constructed. We use this basis to construct globally C^r -smooth geometric mapping that maps the parametric domain $\hat{\Omega}$ to the physical domain Ω with exact recovery of the NURBS bound-

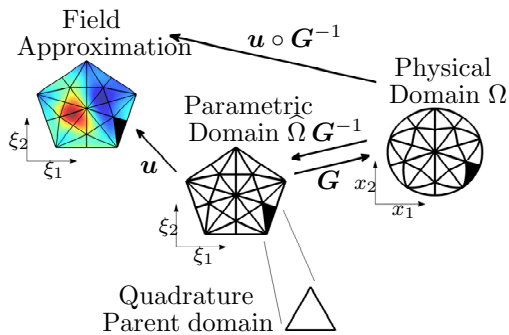


Fig. 1. Isogeometric analysis on triangulations.

ary. When exceptional vertices/edges are allowed, this approach also ensures global bijectivity of the mapping. We demonstrate our analysis results for linear elasticity and advection-diffusion problems on problems which are characteristically non-trivial to mesh by other methods. Since robust technologies for automatic triangulation with local refinement are currently available, our approach is fully automated, is applicable to objects of complex topologies and allows for local refinement during in the course of analysis.

Our work differs from prior work on multivariate-spline based analysis [16][17] in that we explicitly construct C^r -smooth bases and use rational Triangular Bézier Splines (rTBS) to ensure the exact recovery of the NURBS boundary. Our work also differs from the recent developed non-uniform rational Powell-Sabin splines for isogeometric analysis [18][19]. Our approach is more general since general C^r spline spaces are considered. Further, we use Bézier ordinates and the corresponding basis functions to represent PDE solutions. Therefore, our Bézier ordinates based representation has direct geometric interpretation. In contrast, the approach [18][19] uses Powell-Sabin triangles and the corresponding normalized Powell-Sabin B-splines to represent the solutions. However, Powell-Sabin triangles are not unique for a given triangulation although the normalized Powell-Sabin B-splines have nice computational properties such as negativity. Further, our approach is applicable to macroelements or non-macroelements alike and the approach in [18][19] is an macroelement based approach.

Figure 1 gives a schematic overview of our proposed approach. A C^r continuous basis $\psi(\xi)$ is constructed over the parametric domain $\hat{\Omega}$. The basis is used to construct an rTBS based geometric map $\mathbf{G}(\xi)$ so that it maps a point $\xi \in \mathbb{R}^2$ in parametric domain $\hat{\Omega}$ to a point $\mathbf{x} \in \mathbb{R}^2$ in the physical domain Ω . The same basis is also used to approximate physical field $u(\xi)$. Composing the inverse of geometric map and the field approximation, $\mathbf{u} \circ \mathbf{G}^{-1}$, defines a field on the physical domain. Quadrature in analysis integration is performed via local barycentric coordinates on the parent triangle.

The remainder of this paper is organized as follows: Section 2 introduces necessary background concepts; Section 3 presents our discretization method - smooth rTBS-based discretization of the physical domain; Section 4 discusses the details of smooth rTBS-based isogeometric analysis; Section 5 contains our numerical results; In Section 6 we

present our conclusions.

2. Background

In this section we briefly introduce the Bézier curve, non-uniform rational B-splines (NURBS) and triangular Béziers. We then discuss the splines over triangulations and the Clough-Tocher and Powell-Sabin splits. This introduction aims to make the paper self-contained and to clarify notation for subsequent sections. For further reading on Bézier curves, B-splines, and Bézier triangles, see [20], for splines on triangulations see [21], and for isogeometric analysis, see [2].

2.1. Bézier and NURBS curves

CAD geometry is usually defined by a NURBS represented boundary. Each knot span of a NURBS curve corresponds to a Bézier curve. A Bézier curve is defined through Bernstein basis functions. A degree- d Bernstein polynomial is defined explicitly by

$$B_{i,d}(\xi) = \binom{d}{i} \xi^i (1-\xi)^{d-i}, \quad \xi \in [0, 1], \quad (1)$$

where ξ is the parameter. A degree- d Bézier curve is defined in terms of $d+1$ Bernstein basis functions and the corresponding control points $\mathbf{p}_i = (x_{1i}, x_{2i})$ as

$$\mathbf{c}(\xi) = \sum_{i=0}^d \mathbf{p}_i B_{i,d}(\xi). \quad (2)$$

A NURBS curve of degree- d is defined as follows

$$\mathbf{c}(\xi) = \frac{\sum_{i=0}^n N_{i,d}(\xi) w_i \mathbf{p}_i}{\sum_{j=0}^n N_{j,d}(\xi) w_j}, \quad (3)$$

where $\{\mathbf{p}_i\} = (x_{i1}, x_{i2})$ represents the coordinate positions of a set of $i = 0, \dots, n$ control points, $\{w_i\}$ is the corresponding weight, and $\{N_{i,d}\}$ is the degree- d B-spline basis function, defined by a knot vector $\Xi = \{\xi_0, \xi_1, \dots, \xi_{n+d+1}\}$. Through repeated knot insertion, the Bézier representation for each knot span of a NURBS curve can be obtained.

2.2. Bézier Triangles

Bézier triangles are based on bivariate Bernstein polynomials. Let a triangle τ with vertices $\mathbf{v}_1, \mathbf{v}_2, \mathbf{v}_3 \in \mathbb{R}^2$ and the barycentric coordinate of a point $\xi \in \mathbb{R}^2$ with respect to the triangle be $\{\gamma_1, \gamma_2, \gamma_3\}$. A degree- d bivariate Bernstein polynomial is defined as

$$B_{\mathbf{i},d}(\xi) = \frac{d!}{i!j!k!} \gamma_1^i \gamma_2^j \gamma_3^k; \quad |\mathbf{i}| = d, \quad (4)$$

where \mathbf{i} represents a triple index (i, j, k) . A triangular Bézier patch is defined as

$$\mathbf{b}(\xi) = \sum_{i+j+k=d} B_{\mathbf{i},d}(\xi) \mathbf{p}_i, \quad (5)$$

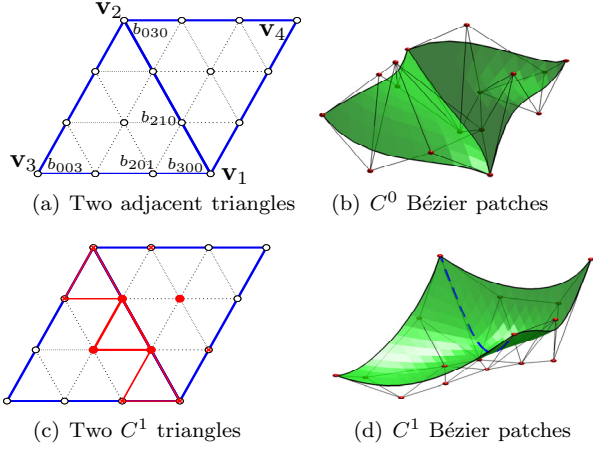


Fig. 2. Triangular Bézier patches and C^1 continuity.

with \mathbf{p}_i represents a triangular array of control points. A rational Bézier triangle can be defined as

$$\mathbf{b}(\boldsymbol{\xi}) = \frac{\sum_{|\mathbf{i}|=d} w_i \mathbf{p}_i B_{\mathbf{i},d}(\boldsymbol{\xi})}{\sum_{|\mathbf{i}|=d} w_i B_{\mathbf{i},d}(\boldsymbol{\xi})}, \quad (6)$$

where w_i are the weights associated with the control points \mathbf{p}_i .

The bivariate Bernstein polynomials can be used to define a polynomial function $f(\boldsymbol{\xi})$ of degree- d over the triangle $\{\mathbf{v}_1, \mathbf{v}_2, \mathbf{v}_3\}$ as:

$$f(\boldsymbol{\xi}) = \sum_{i+j+k=d} b_{ijk} B_{ijk,d}(\boldsymbol{\xi}) \quad (7)$$

where b_{ijk} are Bézier ordinates of $f(\boldsymbol{\xi})$ and the points

$$\mathbf{q}_{ijk} = \frac{i\mathbf{v}_1 + j\mathbf{v}_2 + k\mathbf{v}_3}{d} \quad (8)$$

are domain points. The points $(\mathbf{q}_{ijk}, b_{ijk})$ are control points of the Bernstein-Bézier form of the polynomial function $f(\boldsymbol{\xi})$. By setting one barycentric coordinate to zero and varying the other two, $\boldsymbol{\xi}$ intersects a triangular edge and the bivariate basis reduces to the Bernstein functions (1). The evaluation of a Bézier triangle can be done by the de Casteljau algorithm [20]

$$b_{\mathbf{i}}^r(\boldsymbol{\xi}) = \gamma_1 b_{\mathbf{i}+\mathbf{e}_1}^{r-1}(\boldsymbol{\xi}) + \gamma_2 b_{\mathbf{i}+\mathbf{e}_2}^{r-1}(\boldsymbol{\xi}) + \gamma_3 b_{\mathbf{i}+\mathbf{e}_3}^{r-1}(\boldsymbol{\xi}), \quad (9)$$

where $r = 1, \dots, d$ and $|\mathbf{i}| = d - r$, $\mathbf{e}_1 = (1, 0, 0)$, $\mathbf{e}_2 = (0, 1, 0)$, and $\mathbf{e}_3 = (0, 0, 1)$.

Two polynomials $f(\boldsymbol{\xi})$ and $\tilde{f}(\boldsymbol{\xi})$ join r times differentially across the common edge of two triangles τ and $\tilde{\tau}$ if and only if the following is true [21]

$$\tilde{b}_{\rho,j,k} - \sum_{\mu+\nu+\kappa=\rho} \frac{\rho!}{\mu! \nu! \kappa!} b_{\mu,j+\nu,k+\kappa} \gamma_1^\mu \gamma_2^\nu \gamma_3^\kappa = 0 \quad (10)$$

for all $\rho \leq r$ and $j + k + \rho = d$.

Figure 2 gives an illustration of triangular Bézier patches and continuity constraints. Here the control points $\mathbf{p}_i \in \mathbb{R}^3$. Figure 2a and Figure 2b show two adjacent domain triangles where the two triangles share one edge $\mathbf{v}_1\mathbf{v}_2$ and the corresponding surface patches. Figure 2c and Figure 2d show the C^1 -continuity constraints imposed on the Bézier ordinates and the resulting C^1 patches.

2.3. Splines on triangulations

Consider a parametric domain $\hat{\Omega}$ and its triangulation T , the spline space of piecewise polynomials of degree- d over T is denote as $\mathbb{S}_d^r(T) = \{f \in C^r(\hat{\Omega}) : f|_\tau \text{ is a polynomial of degree } d, \forall \tau \in T\}$, where τ is an arbitrary triangle in T .

To obtain C^r smoothness for any spline, one may simply assert (10) repeatedly and solve the continuity constraints or through macroelement techniques with polynomials of degrees much higher than r or lower degree polynomials based on a split scheme where each triangle in T is split into several micro-triangles. The original triangle is then called a macro-triangle. Splines with higher-order polynomials over each triangle include $d \geq 4r + 1$ [22] and $d \geq 3r + 2$ [23] for general triangulation. However, due to their efficiency C^r -smooth polynomials of lower degree over macro-triangulations are often preferred. These include the Clough-Tocher split [24][25] where one triangle is subdivided into three micro-triangles with polynomials of degree $d = 3r$ for continuity r -odd and $d = 3r + 1$ for r -even, the Powell-Sabin split [26] with polynomials of degree $d = \lfloor \frac{9r+1}{4} \rfloor$ for r -odd, and of degree $d = \lfloor \frac{9r+4}{4} \rfloor$ for r -even, and numerous others [21]. Convenient B-spline-like bases for PS-6 split [27], recently for PS-12 split [28], normalized Clough-Tocher split [29], Quintic PS-splines [30], and a family of PS splines [31] have been proposed.

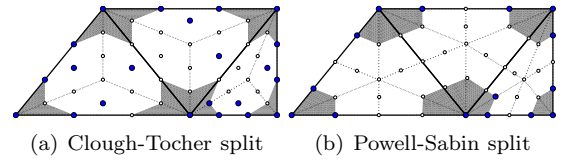


Fig. 3. The Clough-Tocher and Powell-Sabin splits of macro-triangles. Domain points corresponding to free Bézier ordinates are highlighted.

Figure 3 shows the Clough-Tocher (CT) and Powell-Sabin (PS) splits and corresponding C^1 cubic and quadratic free domain points respectively. C^r spaces can be achieved on these splits at elevated degrees [21]. In the Clough-Tocher split, it connects each vertex of a triangle with its incenter to form three micro-triangles. Each micro-triangle is represented by a cubic polynomial. In the Powell-Sabin split, each macro-triangle is split into six micro-triangles with incenter as the interior split point. Edges are then split by joining incenters of adjacent triangles. In practice and in our implementation, the centroid point, instead of the incenter, of each triangle is used in both CT and PS splits and boundary edges are bisected in the PS splits. Besides the CT and PS splits, we perform uniform h -refinement by connecting edge midpoints to subdivide each triangle into four parts. Adaptive refinement is accomplished by the Rivara method [32]. Each subdivision in the Rivara method is an element bisection across one of its edges.

3. Automatic C^r rTBS Domain Parameterization

This section details our method for discretizing a physical domain Ω into a collection of rational Bézier triangles without any geometric-approximation error. Given an arbitrary 2D domain Ω and its NURBS-represented boundary $\Gamma = \cup_i c_i(\xi)$ of degree- d , we seek a geometric map $\mathbf{G}(\boldsymbol{\xi})$, $\boldsymbol{\xi} \in \hat{\Omega}$ such that:

- the physical domain Ω is the image of the geometric map $\mathbf{G}(\boldsymbol{\xi})$ over a parametric domain $\hat{\Omega}$, i.e. $\Omega = \{(x_1, x_2) \in \mathbb{R}^2 : (x_1, x_2) = \mathbf{G}(\boldsymbol{\xi}), \boldsymbol{\xi} \in \hat{\Omega}\}$,
- the boundary of the domain Γ is exactly reproduced by the map $\mathbf{G}(\boldsymbol{\xi})$ at the boundary $\hat{\Gamma}$ of the parametric domain $\hat{\Omega}$, i.e. $\Gamma = \{(x_1, x_2) \in \mathbb{R}^2 : (x_1, x_2) = \mathbf{G}(\boldsymbol{\xi}), \boldsymbol{\xi} \in \hat{\Gamma}\}$, and
- the map is continuous and differentiable up to any desired degree of continuity C^r .

We show how this domain can be decomposed into a set of rational Triangular Bézier patches with C^r inter-patch continuity and exact recovery of domain boundary. We achieve this result in three main steps:

- (i) Construct a geometric map \mathbf{G}_0 based on C^0 Bézier triangles where the input NURBS boundary curves are exactly reproduced. As a by-product of this step, we obtain a polygonal approximation Ω_0 of the physical domain Ω that topologically has the same genus as the physical domain Ω and geometrically approximates the boundary of the domain Γ .
- (ii) Form a polygonal parametric domain $\hat{\Omega}$ from Ω_0 and a triangulation T of $\hat{\Omega}$.
- (iii) Form a C^r basis, $\boldsymbol{\psi}(\boldsymbol{\xi})$, on T and obtain a globally C^r geometric map \mathbf{G} from the parametric domain $\hat{\Omega}$ onto the physical domain Ω , which exactly reproduces the domain boundary.

3.1. Step 1 - Construct a C^0 map \mathbf{G}_0

Our approach to construct an rTBS mesh with exact domain boundary is to approximate the curved domain Ω by a polygon Ω_0 , triangulate $\Omega_0 \rightarrow T$, and then replace the boundary segments of T by segments of the exact NURBS boundary. This process for obtaining a C^0 rTBS mapping \mathbf{G}_0 is accomplished by the following sub-steps (see Fig. 4):

- (a) *Boundary subdivision and Bézier extraction*: Subdivide each NURBS curve $c_i(\xi)$ of degree- d into a set of Bézier curves via knot insertions. The linear segments connecting the resulting Bézier end-points should form a good approximation of the NURBS boundary.
- (b) *Triangulation of the polygonal domain*: The Bézier end-points from Step 1a are connected to form a polygonal domain Ω_0 . The polygonal domain Ω_0 is then triangulated to obtain T_0 .
- (c) *Domain points*: Domain points of degree- d (and coincident control points) for each triangle in T_0 from Step 1b are created based on (8). In this sub-step, the weights

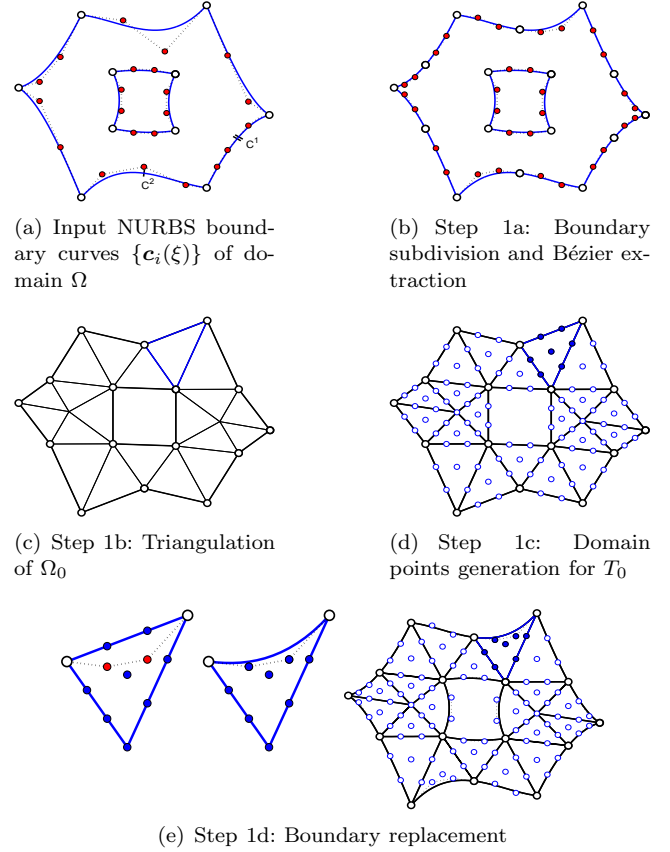


Fig. 4. Constructing boundary conformal C^0 Bézier triangles.

of all Bézier control points are chosen to be unity.

Note that each degree- d Bézier curve segment in Step 1a corresponds to one boundary edge in T_0 , which in turn has $d + 1$ domain points after Step 1c. Thus, each Bézier control point for the domain boundary now corresponds to one domain point on the boundary edge of T_0 .

- (d) *Boundary replacement*: Replacing boundary control points of T_0 with corresponding control points on the Bézier curves in Step 1a to obtain the triangular mesh \mathbf{G}_0 . In this substep, the weights of the boundary Bézier control points are replaced by the weights from the corresponding Bézier points in Step 1a.

Figure 4 illustrates how a domain bounded by NURBS curves $c_i(\xi)$ is decomposed into a collection of C^0 triangular Bézier patches with exact geometry as in $c_i(\xi)$. Figure 4a shows a domain bounded by two sets of cubic, clamped NURBS curves, one an external contour and the other an internal contour. The circular points are control points. The end-points of each NURBS curve are shown in empty circles. Also shown are two sets of ticks that represent internal knots with C^2 and C^1 smoothness on the curves. The first substep shown in Figure 4b is the subdivision of NURBS boundary curves via repeated knot insertions to obtain its Bézier representation. The inserted knots include all of the internal knots from the NURBS boundary as well as additional knots that are inserted so that the re-

sulting polygons connecting the Bézier end points form a good approximation of the given domain Ω bounded by the NURBS curves. Figure 4c shows the resulting polygon Ω_0 and its triangulation T_0 . Figure 4d shows the creation of domain/control points on T_0 so that each triangle becomes a degree-3 Bézier triangle. Figure 4e highlights one triangle in T_0 in Fig. 4d with its boundary control points replaced by boundary Bézier control points from Figure 4b.

Remark 1. *Bézier triangles \mathbf{G}_0 exactly reproduce the NURBS represented domain boundary Γ .*

With the substeps outlined above, the boundary of the Bézier discretization \mathbf{G}_0 of the domain Ω retains all control points of the Bézier-subdivided NURBS boundary $\mathbf{c}_i(\xi)$. That is, we have obtained a triangular discretization of the domain Ω with no approximation error. The C^0 mesh \mathbf{G}_0 of Ω can thus be directly used for analysis where mesh refinement of each Bézier triangle can be conducted without introducing any discretization error from the original geometry. We note that \mathbf{G}_0 alone is sufficient to perform isogeometric analysis with C^0 smoothness between elements. In such analysis, each Bézier patch can be mapped to a canonical triangular domain for integration with the corresponding basis function $\phi(\boldsymbol{\xi})$ defined as the bivariate Bernstein polynomials (4).

3.2. Step 2 - Form a global parametric domain $\widehat{\Omega}$ and its triangulation T

A by-product of the above C^0 rTBS discretization of Ω is its polygonal approximation Ω_0 and triangulation T_0 . In this second step, we present a procedure to form a suitable parametric domain $\widehat{\Omega}$ and triangulation T on which a globally- C^r polynomial basis can reproduce the exact NURBS boundary.

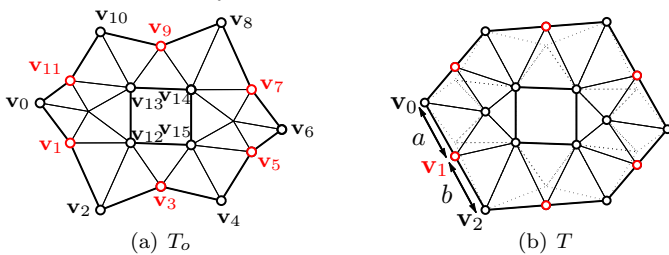


Fig. 5. Adjusting smooth boundary vertices in T_0 to form T .

We obtain the parametric domain $\widehat{\Omega}$ and its triangulation T by adjusting those vertices in T_0 that correspond to knot-points of C^k ($k \geq r$) smoothness in the boundary curves. We move each such boundary vertex to the line segment connecting the adjacent vertices of C^q ($0 \leq q < r$) smoothness. Figure 5 illustrates this process starting from T_0 in Figure 4. Smooth boundary vertices such as $\mathbf{v}_1, \mathbf{v}_3, \dots, \mathbf{v}_{11}$ in Figure 5a must be positioned so that a C^r boundary trace can reproduce the original C^r NURBS segment, as shown in Figure 5b. This implies that the adjusted vertices must be positioned so that the length-ratio of consecutive edges $a = |\mathbf{v}_0\mathbf{v}_1|$ and $b = |\mathbf{v}_1\mathbf{v}_2|$ is the same as the ratio of

the corresponding knot intervals $|t_1 - t_0| : |t_2 - t_1|$ in the boundary NURBS curve.

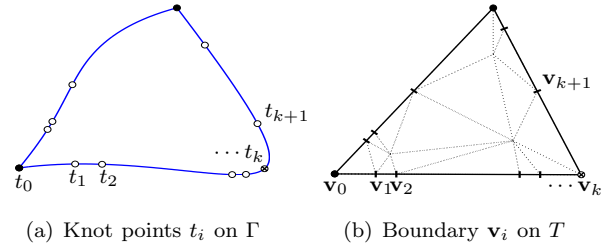


Fig. 6. Smooth knot points in the boundary of Γ may be mapped from a corner vertex \mathbf{v}_k in the parametric domain $\widehat{\Omega}$ to ensure mapping quality.

If too few C^q ($0 \leq q < r$) knot points occur in the boundary to form a suitable domain $\widehat{\Omega}$, additional smooth knot points are used as corner vertices instead. Figure 6 illustrates the formation of a suitable parametric domain from one NURBS curve. In this case, the smooth knot point $\mathbf{c}(t_k)$ is mapped from a corner vertex \mathbf{v}_k , and boundary vertices \mathbf{v}_i with corresponding knot values t_i are arranged to satisfy (11).

$$\begin{aligned} & |\mathbf{v}_0\mathbf{v}_1| : |\mathbf{v}_1\mathbf{v}_2| : \dots : |\mathbf{v}_{k-1}\mathbf{v}_k| \\ & = (t_1 - t_0) : (t_2 - t_1) : \dots : (t_k - t_{k-1}) \end{aligned} \quad (11)$$

Note, if a degree- d NURBS curve has knots with multiplicity m such that $d - m < r$, i.e. the smoothness at the knots is lower than C^r , the basis functions at the corresponding parametric locations thus cannot be C^r smooth if exact recovery of NURBS boundary is to be enforced. Knots of lower-order continuity are therefore mapped from corner vertices with non-collinear adjacent boundary edges in the parametric domain.

We further assume that a *stable local spline space* [21] $\mathbb{S}_d^r(T)$ can be defined on T . That is, apart from asserting C^0 continuity at parametric domain corners, we can assume that basis functions with support intersecting one edge of $\widehat{\Omega}$ are independent of those intersecting another. The boundary of the triangulation now has the following property:

Theorem 1 *For spline space $\mathbb{S}_d^r(T)$, the space of boundary traces along the domain boundary $\widehat{\Gamma}$ is a set of closed univariate degree- d B-splines with C^r smoothness at each straight boundary vertex and C^0 for corner boundary vertices. Each knot span of the univariate B-splines has its length proportional to the length of corresponding linear segment in $\widehat{\Gamma}$.*

3.3. Step 3 - Form a C^r spline basis $\psi(\boldsymbol{\xi})$ on T

Let $\mathcal{D}_{d,T}$ denote the set of domain points of degree- d for triangulation T , $\mathbf{v} \in \mathcal{D}_{d,T}$ a domain point and $b_{\mathbf{v}}$ its ordinate. The C^r smoothness conditions (10) among Bézier ordinates imply the existence of a reduced set of domain points $\mathcal{M}_{d,T} \subset \mathcal{D}_{d,T}$ whose Bézier ordinates, when freely specified, uniquely determine the remaining ordinates. This reduced set of *free-nodes* is called a *Minimum Determining*

Set (MDS) [21][33]. We define a basis $\psi(T)$ for the spline space $\mathbb{S}_d^r(T)$ in terms of these free-nodes as:

$$\psi(T) = \{\psi_{\mathbf{v}} \in \mathbb{S}_d^r(T) : \mathbf{v} \in \mathcal{M}_{d,T}, b_{\mathbf{v}} = 1, \\ b_{\mathbf{u}} = 0, \forall \mathbf{u} \neq \mathbf{v} \in \mathcal{M}_{d,T}\}$$

We describe below how to construct ψ from a given triangulation T and how a free-node distribution can be chosen to allow us to directly specify a NURBS boundary.

3.3.1. Boundary minimum determining set $\mathcal{M}_{d,\hat{\Gamma}}$

To facilitate later discussion we extend the MDS concept from above to define the *Boundary MDS* $\mathcal{M}_{d,\hat{\Gamma}}$ for the domain boundary $\hat{\Gamma}$ as a minimum set of domain points along the boundary whose ordinates uniquely specify its trace.

Among the set of all the domain points $\mathcal{D}_{d,\Gamma}$ along the boundary of $\hat{\Gamma}$ subject to the localization condition of §3.2, every C^r -smooth vertex is subject to r linear equations (10). Thus for every C^r -smooth vertex, exactly r Bézier ordinates must be determined from the other ordinates. Following the MDS concept in [21][33], we refer to these free ordinates as a minimal determining set for the domain boundary.

A Boundary MDS for the domain in Figure 4 is indicated for the triangulation T in Figure 8(a).

3.3.2. C^r spline basis $\psi(\xi)$ via MDS $\mathcal{M}_{d,T}$

The continuity constraints (10) essentially amount to a homogeneous linear system

$$\mathbf{A}\mathbf{b}_{\mathcal{D}} = \mathbf{0} \quad (12)$$

where \mathbf{A} is a coefficient matrix depending on the geometry of the domain triangles and $\mathbf{b}_{\mathcal{D}}$ are n Bézier ordinates for the corresponding domain points $\mathcal{D}_{d,T}$. The i -th row of \mathbf{A} corresponds to the coefficients in the Bézier ordinates of the i -th constraint and the j -th column in \mathbf{A} corresponds to the Bézier ordinate b_j . The dimension of the space $\mathbb{S}_d^r(T)$ is $\dim \mathbb{S}_d^r(T) = \dim \mathbb{S}_d^0(T) - \text{rank}(\mathbf{A})$.

With the linear continuity constraints among the Bézier ordinates, only a subset of these ordinates can be free while the others are determined. For the given linear system $\mathbf{A}\mathbf{b}_{\mathcal{D}} = \mathbf{0}$, through Gauss-Jordan elimination with pivoting (eg: row-wise partial pivoting) to match ordinates with their governing constraints, where both items below and above diagonal terms are zeroed, we obtain the following equation

$$\begin{bmatrix} \mathbf{I}_{(n-m) \times (n-m)} & \mathbf{R}_{(n-m) \times m} \\ \mathbf{0}_{m \times (n-m)} & \mathbf{0}_{m \times m} \end{bmatrix} \begin{bmatrix} \mathbf{b}_{(n-m) \times 1}^d \\ \mathbf{b}_{m \times 1}^f \end{bmatrix} = \mathbf{A}\mathbf{b}_{\mathcal{D}_{d,T}} = \mathbf{0}. \quad (13)$$

In the above equation, we obtain $n - m$ Bézier ordinates \mathbf{b}^d that can be expressed as functions of m free ordinates \mathbf{b}^f :

$$\mathbf{b}_{(n-m) \times 1}^d = -\mathbf{R}_{(n-m) \times m} \mathbf{b}_{m \times 1}^f. \quad (14)$$

The m free Bézier ordinates \mathbf{b}^f correspond to the domain points in $\mathcal{M}_{d,T}$. We denote these ordinates as $\mathbf{b}_{\mathcal{M}_{d,T}}$. Defin-

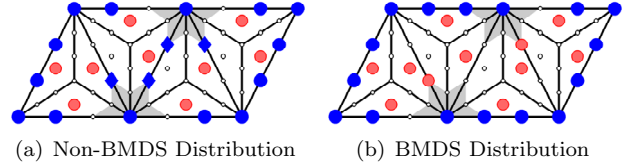


Fig. 7. Adjusting free nodes to form a boundary MDS. Free nodes are shown with solid markers, and constrained nodes by small circles. Free nodes with influence on the boundary are further darkened. In (a) the two internal free nodes shown as diamonds have influence on the boundary. A boundary MDS is formed in (b) by moving one of these free nodes to the boundary.

ing the augmented matrix $\mathbf{C} = \begin{bmatrix} -\mathbf{R}_{(n-m) \times m} & \mathbf{I}_{n-m \times n-m} \end{bmatrix}$, we have

$$\mathbf{b}_{\mathcal{D}_{d,T}} = \mathbf{C}^T \mathbf{b}_{\mathcal{M}_{d,T}}, \quad (15)$$

where the \mathbf{C} matrix transforms the Bézier ordinates in $\mathcal{M}_{d,T}$ to ordinates in $\mathcal{D}_{d,T}$.

In order to apply Dirichlet conditions and to specify a NURBS boundary, we could use a set of Lagrange multipliers as used in [16][17] to enforce boundary conditions. However, by requiring our MDS to contain a valid Boundary MDS (16) we are able to explicitly impose these conditions.

$$\mathcal{M}_{d,\hat{\Gamma}} \subset \mathcal{M}_{d,T}. \quad (16)$$

A Boundary MDS can be enforced by shifting columns $\mathcal{M}_{d,T}$ of \mathbf{A} to the end during initial pivoting, or after Gauss-Jordan elimination, by exchanging any free-node with influence on the boundary with a constrained boundary node. A free-node appears in \mathbf{C} as a column with a single 1 that is otherwise all zeros. If a constrained boundary node is dependent on a free internal node, then by scaling this free basis row, and adding multiples of it to zero the boundary node's column, we replace the internal free-node by one on the boundary (Figure 7). If all such cases are adjusted, then the complete boundary will be uniquely determined by its boundary free-nodes so giving us a boundary MDS.

An arbitrary piecewise polynomial function $f(\xi) : \xi \in T$ can be expressed in terms of the C^0 Bernstein Basis ϕ_i and corresponding nodal ordinates $b_{\mathcal{D}}$ as:

$$f(\xi) = \sum_i b_i \phi_i(\xi) = \mathbf{b}_{\mathcal{D}}^T \phi(\xi) \quad (17)$$

If f is further C^r -continuous, by (15), it can be expressed equivalently in terms of its free nodal ordinates $b_{\mathcal{M}}$ as:

$$f(\xi) = \mathbf{b}_{\mathcal{D}}^T \phi(\xi) = \mathbf{b}_{\mathcal{M}}^T \mathbf{C} \phi(\xi) = \mathbf{b}_{\mathcal{M}}^T \psi(\xi). \quad (18)$$

That is, we have constructed the globally C^r basis functions $\psi(\xi) = \mathbf{C} \phi(\xi)$ as a linear combination of the C^0 Bernstein basis $\phi(\xi)$.

3.3.3. Exceptional vertices

It may occur that a NURBS knot-point on the domain boundary is no more than C^k smooth for some $k < r$. In this case, by the method of §3.2 a corner of the parametric domain must be aligned with the knot point to ensure exact boundary representation. However, if the point is at least G^1 smooth this results in a loss of bijectivity at that point.

When global bijectivity is desired we amend our method as follows: In §3.2 we align corners of our polygon only with C^0 knot-points and any others needed to form a suitable polygonal domain. Around each of these latter vertices and those aligned with C^k knot-points for $k < r$ we further select an internal macro-element edge across which to reduce continuity. We do this by removing constraints from \mathbf{A} that bridge the edge, involve the vertex node, and are required to assure C^{k+1}, \dots, C^r continuity. We call these *exceptional vertices* and *exceptional edges*. An example is shown in Figure 16c and Figure 18 where four exceptional vertices and respectively four exceptional edges are used to reduce continuity around the vertices/edges to avoid singularity in geometric mapping. As the model is refined, the exceptional edges become shorter. Such trading the local reduction of continuity for improvement of mesh quality can be especially beneficial in analysis, as demonstrated in Figure 18.

Proposition 1 *A globally bijective map \mathbf{G} can be obtained for any domain Ω after exceptional vertex insertion and uniform refinement.*

3.4. Geometric map $\mathbf{G}(\boldsymbol{\xi})$

We now have a coarse boundary-conformal Bézier mesh \mathbf{G}_0 and parametric triangulation T of the corresponding domain $\hat{\Omega}$. While mesh refinements may be performed by inserting knot-points into the boundary before Step 1, or after Step 1, they can be performed as late as after generating T . Whatever optional mesh refinements take place, in order to form a C^r spline basis on our mesh (in particular the Clough-Tocher or Powell-Sabin splines), the final stage of refinement after forming T must be its corresponding split. The subdivision of rTBS elements are topologically similar to the split as performed in the barycentric domain of each element [34] (See Figure 12). On the boundary, parametric equivalence between the rTBS subdivision and domain subdivision are strictly maintained. The interior control points for rTBS elements are overridden by a subset of free control points under C^r constraints, and they provide a reference for C^r mesh quality (see Section 5.1.1). Any refinements after forming T must be applied in parallel to \mathbf{G} and T to maintain index correspondence between domain points in T and control points for \mathbf{G}_0 .

With the C^r basis $\boldsymbol{\psi}(\boldsymbol{\xi})$ and domain points in the MDS $\mathcal{M}_{d,T}$, we can now obtain the geometric map $\mathbf{G}(\boldsymbol{\xi})$ in terms of the constructed C^r basis functions $\boldsymbol{\psi}_j : \hat{\Omega} \rightarrow \mathbb{R}$, or equivalently, the C^0 Bernstein basis functions $\phi_i : \hat{\Omega} \rightarrow \mathbb{R}$, in the form

$$\mathbf{G}(\boldsymbol{\xi}) = \frac{\sum_i^m w_i \mathbf{p}_i \psi_i(\boldsymbol{\xi})}{\sum_i^m w_i \psi_i(\boldsymbol{\xi})}. \quad (19)$$

where $\mathbf{p}_i = (x_1, x_2)_i$ are control points corresponding to domain points \mathbf{q}_i in $\mathcal{M}_{d,T}$, and w_i are the weights for the corresponding control points. Combining \mathbf{p}_i and w_i in the homogeneous form as $(w_i x_{1i}, w_i x_{2i}, w_i)$, we can obtain the map in homogeneous coordinates as

$$\mathbf{G}^{(W)}(\boldsymbol{\xi}) = \mathbf{P}_{\mathcal{M}}^{(W)T} \boldsymbol{\psi}(\boldsymbol{\xi}) = \mathbf{P}_{\mathcal{M}}^{(W)T} \mathbf{C} \boldsymbol{\phi}(\boldsymbol{\xi}) = \mathbf{P}_{\mathcal{D}}^{(W)T} \boldsymbol{\phi}(\boldsymbol{\xi}). \quad (20)$$

Then,

$$\mathbf{C}^T \mathbf{P}_{\mathcal{M}}^{(W)} = \mathbf{P}_{\mathcal{D}}^{(W)}. \quad (21)$$

That is, we can obtain control points of all the domain points $\mathbf{P}_{\mathcal{D}}^{(W)}$ from those $(\mathbf{P}_{\mathcal{M}}^{(W)})$ of MDS.

The control points corresponding to boundary MDS $\mathcal{M}_{d,\Gamma}$ in the geometric map $\mathbf{G}(\boldsymbol{\xi})$ are a subset of Bézier control points of the input NURBS curves. These control points can then be used to explicitly determine the boundary ordinates of $\mathbf{P}_{\mathcal{M}}^{(W)}$ and so $\mathbf{P}_{\mathcal{M}}$. Subject to the conditions of Theorem 1 we thus have the following proposition:

Proposition 2 *The NURBS curves $\mathbf{c}_i(\boldsymbol{\xi})$ in the boundary Γ can be exactly reproduced by the geometric map $\mathbf{G}(\boldsymbol{\xi})$ with the smooth basis $\boldsymbol{\psi}(\boldsymbol{\xi})$ in $\mathbb{S}_d^r(T)$.*

Figure 8 shows an rTBS discretization of the domain from Figure 4 with Clough-Tocher split and one composed C^1 basis function $\boldsymbol{\psi}(\mathbf{x}) = \boldsymbol{\psi}(\boldsymbol{\xi}) \circ \mathbf{G}^{-1}(\mathbf{x})$.

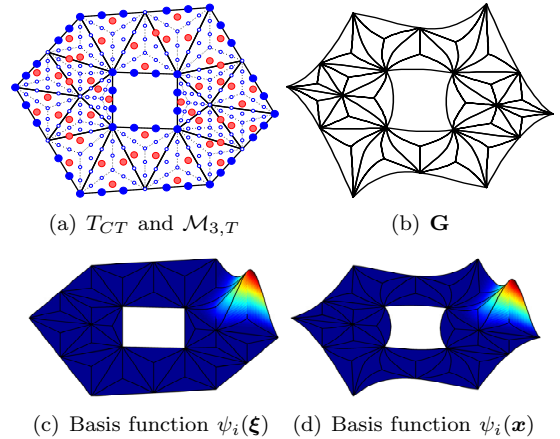


Fig. 8. rTBS discretization of the domain in Figure 4 with CT split, free boundary (darkened) and internal (light) nodes (a), and basis functions $\boldsymbol{\psi}_i(\boldsymbol{\xi})$ and $\boldsymbol{\psi}_i(\mathbf{x})$.

4. Isogeometric Analysis through rTBS Elements

In this section, we describe the basic procedure for isogeometric analysis with C^0 and C^r triangular Bézier elements. Our approach is based on the Bézier mesh \mathbf{G}_0 for C^0 elements and \mathbf{G} and T triangulation for C^r analysis. The C^r basis functions $\boldsymbol{\psi}(\boldsymbol{\xi})$ and C^0 basis functions $\boldsymbol{\phi}(\boldsymbol{\xi})$ are respectively used for C^r and C^0 elements. However, using the linear relationship $\boldsymbol{\psi}(\boldsymbol{\xi}) = \mathbf{C}^T \boldsymbol{\phi}(\boldsymbol{\xi})$ and (9), integration can be done over the finest level of triangles $\tau \in T$.

In this paper, we solve several linear partial differential equations including linear elasticity and advection-diffusion analysis. For linear elasticity, the strong form is

$$\nabla_s^T \boldsymbol{\sigma} + \mathbf{b} = 0, \quad (22)$$

with displacement boundary condition $\mathbf{u} = g_D$ on Γ_D and traction $\boldsymbol{\tau} \mathbf{n} = g_N$ on Γ_N . In advection-diffusion analysis, the following boundary-value problem is solved to deter-

mine the steady-state distribution of a substance propagated by a moving fluid

$$-\nabla\kappa\nabla u + \mathbf{a} \cdot \nabla u = 0 \text{ in } \Omega \quad (23)$$

with Dirichlet conditions on Γ_D and Neumann conditions on Γ_N . Here, κ is the diffusion coefficient of the substance and \mathbf{a} is the local fluid velocity.

Converting the above strong forms of PDEs into their weak forms, and discretizing these weak forms lead to a set of linear algebraic equations. For more details on such finite element methods, we refer the reader to any introductory textbook on finite element methods [35][36]. In this paper, we apply the Galerkin formulation where test functions and the approximate solution are built from the basis constructed in the previous section. That is, we approximate the solution in the parametric domain as

$$\hat{u}(\boldsymbol{\xi}) \approx \sum_i u_i \psi_i(\boldsymbol{\xi}) = \mathbf{u}^T \boldsymbol{\psi} \quad (24)$$

where u_i corresponds to the approximate solution's Bézier ordinate at the domain point i in parametric domain $\hat{\Omega}$'s triangulation T . We can obtain the solution $u(\mathbf{x})$ in the physical space by composing its representation $\hat{u}(\boldsymbol{\xi})$ in the parametric domain with the inverse of the geometrical mapping G^{-1} so that $u : \Omega \rightarrow R$ is obtained by

$$u(\mathbf{x}) = \hat{u} \circ \mathbf{G}^{-1}(\mathbf{x})$$

where \mathbf{G} can be \mathbf{G}_0 or \mathbf{G}_1 for C^0 and C^r elements respectively. Figure 9 illustrates the distribution of free-nodes governing a shaded C^0 , C^1 Powell-Sabin and C^1 Clough-Tocher element. Figure 9a highlights the domain points with non-vanishing basis functions over the shaded C^0 triangular element. Figures 9b and c respectively highlight free-nodes with non-vanishing basis functions over a Powell-Sabin and Clough-Tocher micro-element. Notably, the same local basis governs all micro-elements of one stable macro-element.

Inserting the basis functions ϕ and the approximate solution (24) into the weak forms and assembling the linear system leads to the following integrals, respectively for stiffness, mass, and advection matrices

$$(\nabla\phi_j, \nabla\phi_i)_\Omega, \quad (\phi_j, \phi_i)_\Omega, \quad (\mathbf{a} \cdot \nabla\phi_j, \phi_i)_\Omega \quad (25)$$

for C^0 elements where j and i correspond to domain control points in C^0 Bézier elements as shown in Figure 9a. Note $(a, b)_\Omega = \int_\Omega ab \, d\Omega$. For C^r elements, we have

$$(\nabla\psi_j, \nabla\psi_i)_\Omega, \quad (\psi_j, \psi_i)_\Omega, \quad (\mathbf{a} \cdot \nabla\psi_j, \psi_i)_\Omega \quad (26)$$

where j and i correspond to free domain points in C^r elements as shown in Figure 9b and Figure 9c.

The numerical integrations of (25) and (26) are performed via quadrature over each domain triangle or boundary edge. For example, element (j, i) of the stiffness matrix is obtained as

$$(\nabla\psi_j, \nabla\psi_i)_\Omega \approx \sum_{\tau \in T} \sum_k w_k |J_G(\boldsymbol{\xi}_k)| (\nabla\psi_i(\boldsymbol{\xi}_k) \cdot \nabla\psi_j(\boldsymbol{\xi}_k)) \quad (27)$$

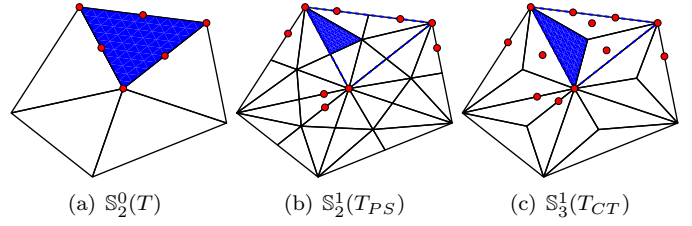


Fig. 9. Free nodes of one element in C^0 rTBS, Powell-Sabin and Clough-Tocher splines.

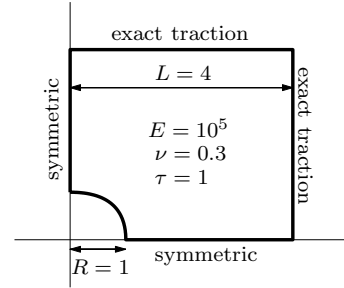


Fig. 10. The plate-hole problem statement.

where τ is a micro-triangle within a macro triangle in T , w_k is the quadrature weight, and J_G is the Jacobian of the geometric mapping. Due to the local support of our spline basis, this stiffness matrix is sparse. For example, with $\mathcal{O}(10^3)$ dof of the quadratic and cubic basis functions of Example 1 showed on average 10 and 16 interactions respectively in the C^0 case and 18 and 23 interactions in the C^1 case. Note, however, that these results will vary depending on the specific triangulation and method of pivoting and basis used in §3.3.2. Basis functions with support at a given node ν can be identified as rows μ of the continuity matrix \mathbf{C} with non-zero entries in column ν .

The Dirichlet boundary conditions can be imposed in a similar way as in NURBS-based isogeometric analysis [2] since the trace of the parametric domain $\hat{\Omega}$ is a just a degree- d B-spline curve with C^0 smoothness at corner vertices and C^r at smooth vertices. That is, one simply projects the Dirichlet conditions into the degree- d B-spline space with knots as per on Theorem 1, and then extracts the Bézier ordinates corresponding to the free-nodes in the Boundary MDS $\mathcal{M}_{d,\Gamma}$.

5. Applied Problems

In this section, we demonstrate rTBS-based isogeometric analysis of linear elasticity and advection-diffusion problems. We demonstrate the effect of incorporating both C^r continuity and adaptive refinement in the analysis of the well-known linear elastic plate-hole problem and the advection-diffusion problem of complex topologies.

5.1. Example 1: Linear elasticity

We apply our approach to a well-known linear elasticity problem: an infinite plate with a hole of radius 1 is subject

to constant in-plane tension at infinity [2]. The problem definition is in Figure 10. The exact solution for this problem is known from [37] and is used to quantify our analysis error. For an error measure we use the L_2 measure of strain energy error, $\Delta(\boldsymbol{\sigma} \cdot \boldsymbol{\epsilon})(\mathbf{x})$. We also use this measure on an element-wise basis to guide adaptive refinement by the Rivara method [32].

5.1.1. *rTBS discretization and mesh smoothing*

For a given element type, the analysis accuracy and convergence rate depend on element quality. In this paper, thus far, we have focused on presenting a set of steps for establishing an rTBS-based geometric map $\mathbf{G}(\boldsymbol{\xi})$ that can exactly recover the given NURBS boundary. However, the interior of the geometric map that directly affects the rTBS element quality has not been explicitly addressed. We here briefly describe how we use smoothing to improve the mesh quality. A formal study of mesh quality and convergence rate is outside of the scope of this paper.

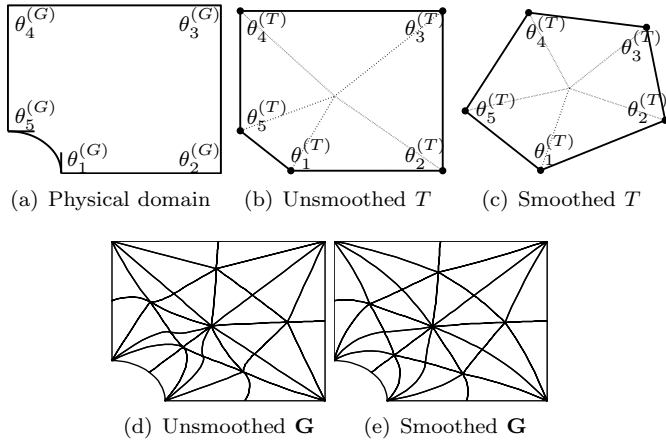


Fig. 11. The smoothing technique is used for the Plate-hole mesh (Example 1). By adjusting the triangulation T (before PS-refinement), we can improve the element shape quality of the output \mathbf{G} .

The factors that can be adjusted to affect mesh quality include the internal control points of \mathbf{G}_0 in Step 1, the free internal control points for \mathbf{G} , and the internal and corner boundary vertex positions of T in Step 2. For the internal control points \mathbf{P}_{0_I} of \mathbf{G}_0 we apply Laplacian smoothing on the Bézier control net of \mathbf{G}_0 . The free internal control points \mathbf{P}_I corresponding to internal domain points in the MDS $\mathcal{M}_{d,T}$ can be freely chosen to improve the mapping quality. Note $\mathbf{P}_M = \mathbf{P}_B \cup \mathbf{P}_I$. Here we simply choose these free internal control points \mathbf{P}_I so that the Bézier control points $\mathbf{C}^T \mathbf{P}_M^W$ for $\mathbf{G}(\boldsymbol{\xi})$ are as close as possible to the control points \mathbf{P}_0^W for \mathbf{G}_0 in the least-squares sense, i.e.

$$\min_{\mathbf{P}_I} |\mathbf{P}_0^W - \mathbf{C}^T \mathbf{P}_M^W|. \quad (28)$$

As for internal and corner boundary vertices, we have observed that the smoothness of the geometric map \mathbf{G} is improved if the internal corner angles $\theta_i^{(T)}$ of T (see Figures 11b and d) approximate the corresponding boundary angles $\theta_i^{(G)}$ of \mathbf{G} (see Figure 11a). This is achieved by freely

varying the corner vertex positions \mathbf{v}_i of T (shown in Figures 11b and d) to minimize the angle difference.

$$\min_{\mathbf{v}_i} f(\hat{\Omega}) = \sum_i |\theta_i^{(T)} - \theta_i^{(G)}|. \quad (29)$$

Remaining boundary vertices in T are then determined based on (11), and internal vertices in T are determined by Laplacian smoothing. This process is performed immediately after Step 2 but before mesh refinement. The result is illustrated in Figure 11e. Figure 12 shows the entire process of obtaining rTBS discretization of the plate-hole domain with Powell-Sabin split and one C^1 basis $\psi(\mathbf{x})$.

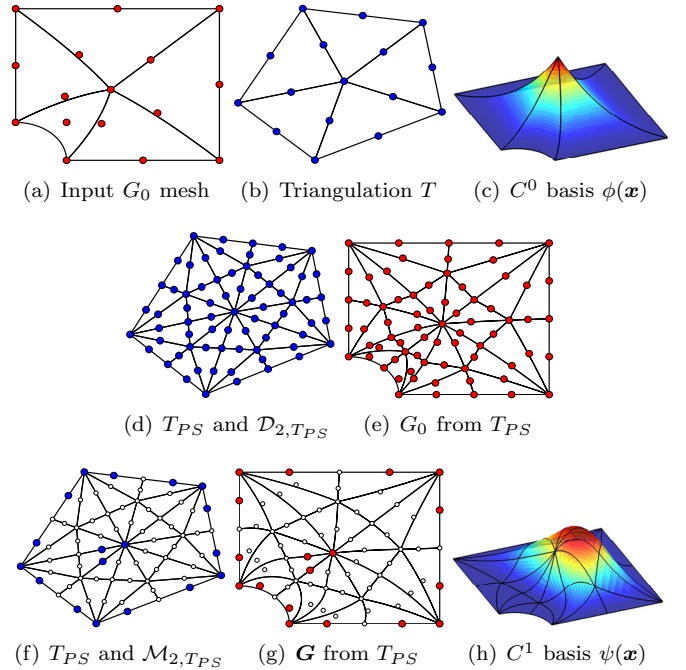


Fig. 12. rTBS discretization with PS split and C^1 basis $\psi(\mathbf{x})$.

5.1.2. *Example 1: Convergence study*

In our convergence study, we use the parametric domain T shown in Figure 11c as produced by our mesh smoothing algorithm. Since this domain has five corners, a NURBS parameterization of this domain either requires the domain to be split by a C^0 knot curve, or requires two control points to lie atop each other, resulting in a singularity in the mapping. In contrast, by using an rTBS mesh with a polygonal parametric domain, we can form a globally C^1 -smooth basis on this domain.

By performing uniform or adaptive h -refinement and p -refinement, we can increase the number of degrees of freedom (DOF) used for analysis. Figure 13 shows the C^0 rTBS elements in spline space $\mathbb{S}_2^0(T)$ and C^1 rTBS elements via Powell-Sabin splits in $\mathbb{S}_2^1(T_{PS})$ under uniform and adaptive h -refinement. The corresponding convergence data for uniform and adaptive refinement are shown in Figure 15a. The convergence rate of the L_2 norm of the energy error over the DOF is shown in the legend of each curve.

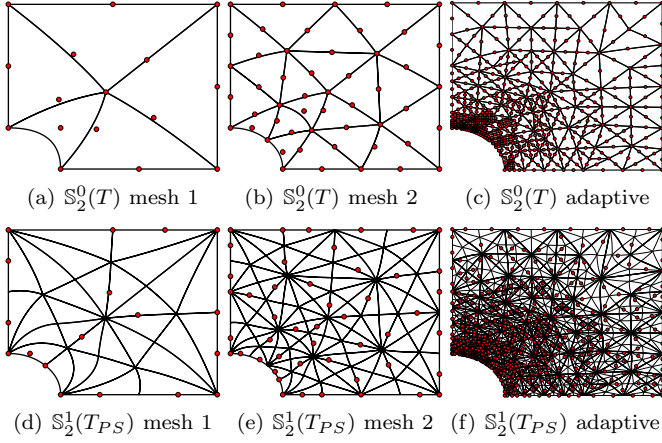


Fig. 13. Quadratic rTBS mesh under uniform and adaptive refinement. Highlighted red points are free nodes.

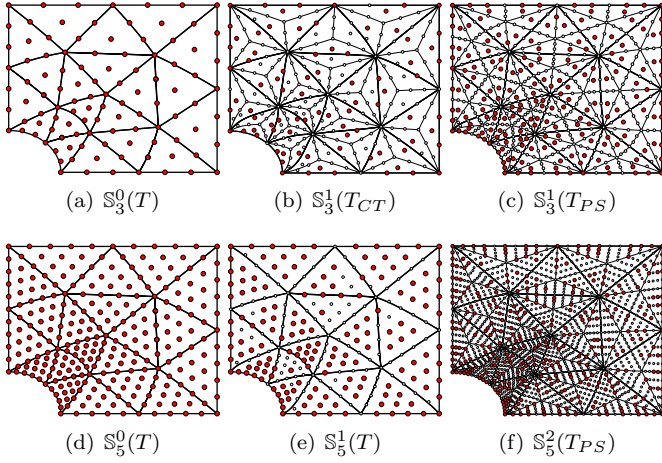
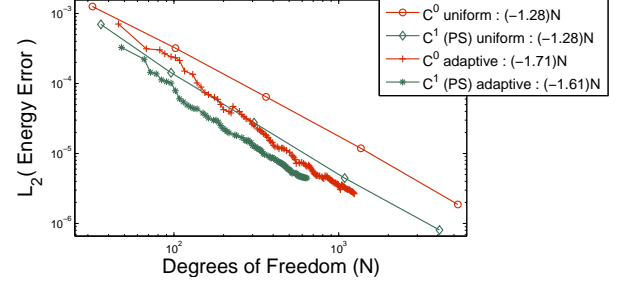


Fig. 14. Cubic and quintic elements. Highlighted points are free nodes.

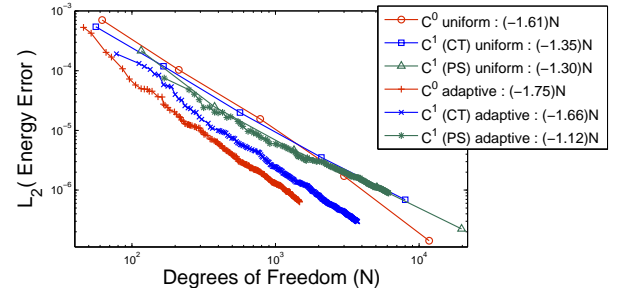
After degree-elevating \mathbf{G}_0 to a cubic mesh, we can form a C^1 basis using either the Clough-Tocher or the Powell-Sabin splits. Free-node distributions for these meshes as compared with the simple C^0 rTBS case are shown in Figures 14a through c, and convergence data are shown in 15b. By degree-elevating \mathbf{G}_0 to a quintic mesh (Figure 14d) we can achieve a stable C^1 basis without performing any further macro-element splits (Figure 14e). Alternatively, by using a Powell-Sabin split we can achieve a C^2 rTBS basis for our domain. Convergence data comparing quintic C^0 , C^1 and C^2 bases are shown in Figure 15c. The condition numbers for the stiffness matrix for splines in Fig. 13(b) and (c) and in Fig. 14 are respectively $5.12e3$, $1.91e4$, $5.42e3$, $1.37e4$, $7.06e3$, $5.66e3$, $1.25e4$ and $2.76e4$.

These convergence results demonstrate that first, when C^0 continuity is used, our method of automatic and adaptive C^0 rTBS meshing leads to nice convergence behaviours. Second, when C^1 continuity is required, we have shown that the quadratic Powell-Sabin, cubic Clough-Tocher, and quintic unstructured splines all converge nicely. Third, although preliminary results show that C^2 rTBS-based analysis does not perform as well compared with C^0 and C^1

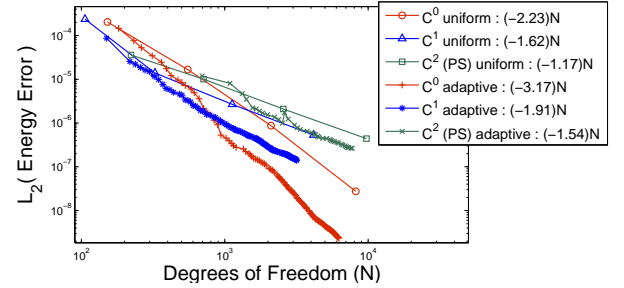
rTBS-based IgA by our method, we have shown that C^2 rTBS-based analysis is viable. Future work will investigate the optimal convergence rate of high-order continuous rTBS-based analysis.



(a) Quadratic elements



(b) Cubic elements



(c) Quintic elements

Fig. 15. Convergence rates for elements in Figure 13 and 14 for the plate-hole problem.

5.2. Example 2: Advection-diffusion

In this example (see Figures 16 and 19) we demonstrate the automatic C^1 meshing and analysis of a genus-1 and a genus-4 domain by applying the stabilized Streamline Upwind Petrov-Galerkin (SUPG) method to solve advection-diffusion problems. The inner boundary is held at $u = 1$ and the outer boundary at $u = 0$. The domain is then subject to a constant flow \mathbf{a} to the right, and a low diffusion coefficient κ . The anticipated shear boundary layers are shown as red-dashed lines in this figure.

Figure 16 details the process of obtaining C^0 and C^1 rTBS discretization of the genus 1 domain. The inner circle is mapped to a quadrilateral corresponding to four rational Bézier curves in Figures 16c. Figures 16d and Figures 16e highlight the local refinement along the flow boundaries. The Powell-Sabin split is used to obtain a quadratic C^1

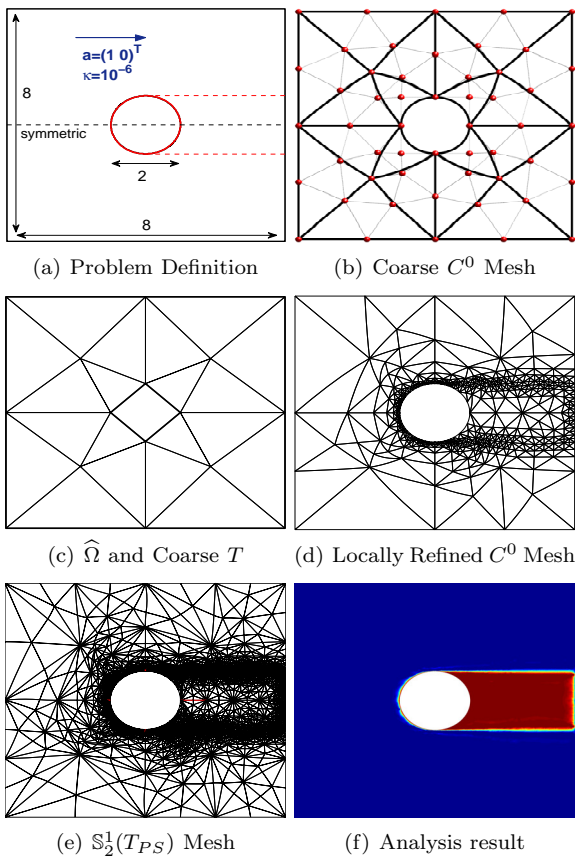


Fig. 16. Isogeometric analysis of the advection-diffusion problem.

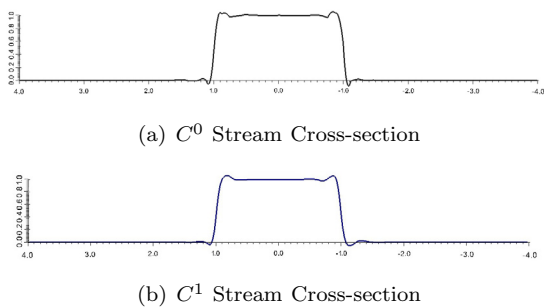


Fig. 17. Solution cross-sections at $x = 2$.

basis, and to avoid singularity in the C^1 mapping \mathbf{G} , four exceptional edges are introduced (shown as red in Figures 16e) in the resulting triangulation T . Figure 17 shows the solution at cross-sections ($x = 2$) from equivalent C^0 and C^1 macroelement meshes. It can be seen that C^0 solution has sharp features while C^1 solution is smooth and is free from high frequency noise. Figure 18 compares the analysis result from globally C^1 mesh without (Figure 18a) and with exceptional edges (Figure 18b). As shown in the inset in Figure 18a, without exceptional edges there is singularity in the geometric mapping and more visible oscillation in the solution. The analysis mesh is obtained from uniform refinement as shown in Figure 18c, Figure 18d and Figure 18e. It can be seen that exceptional edges are receding and becoming shorter during the refinement.

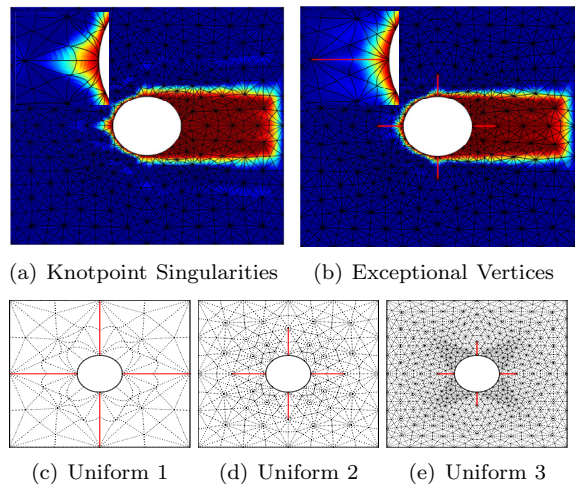


Fig. 18. Uniformly refined analysis results show the effects of knotpoint singularities (a), and exceptional vertices/edges (b) (edges indicated in red). Exceptional edges recede on refinement (c,d,e).

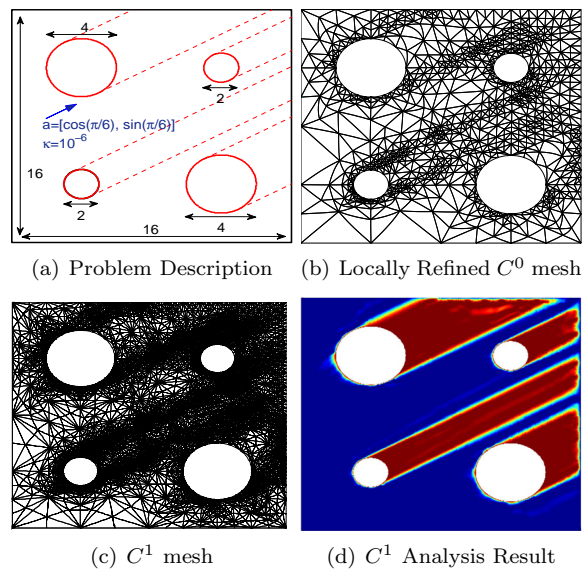


Fig. 19. Isogeometric meshing and analysis for a genus 4 domain.

The isogeometric meshing and analysis of the genus-4 domain are shown in Figure 19. After local refinement of \mathbf{G}_0 to resolve shear boundary layers (Figure 19b), uniform refinement by the Powell-Sabin split, and performing the projections of Step 3, then the rTBS mesh (shown in Figure 19c) is constructed. In Figure 19c, 16 exceptional vertices with 4 for each circle are introduced. The resulting analysis field is again globally bijective and C^1 smooth except in the immediate vicinity of each exceptional vertex.

6. Conclusions

We have presented a new isogeometric analysis approach based on rational Triangular Bézier Splines (rTBS). The rTBS parametrization of a NURBS-bounded domain can be fully automated. This approach is applicable to complex topologies. Various local refinement schemes can be read-

ily implemented. We have presented a set of procedures for constructing a globally C^r -continuous basis for representing both physical field and the domain geometry with exact recovery of its NURBS boundary. We have also introduced the concept of exceptional vertices/edges where a reduced set of continuity constraints is imposed at boundary vertices. The reduced continuity at exceptional vertices and edges leads to global bijectivity and improved mesh quality and analysis results. Unlike tensor-product NURBS, such reduced continuity becomes highly localized with mesh refinement. This rTBS-based isogeometric analysis has been shown to be convergent with mesh refinement on linear elasticity and advection-diffusion problems.

Future work will focus on improving rTBS element quality to achieve optimal convergence rate, studying the nestedness of spline space, and extending this approach to three-dimensional problems.

References

- [1] T. J. R. Hughes, J. A. Cottrell, and Y. Bazilevs. Isogeometric analysis: CAD, finite elements, NURBS, exact geometry and mesh refinement. *Computer Methods in Applied Mechanics and Engineering*, 194(39):4135–4195, 2005.
- [2] J. A. Cottrell, T. J. R. Hughes, and Y. Bazilevs. *Isogeometric analysis: Toward integration of CAD and FEA. 2009*. John Wiley & Sons.
- [3] M. Aigner, C. Heinrich, B. Jüttler, E. Pilgerstorfer, B. Simeon, and A. Vuong. Swept volume parameterization for isogeometric analysis. *Mathematics of Surfaces XIII*, pages 19–44, 2009.
- [4] T. Martin, E. Cohen, and R. M. Kirby. Volumetric parameterization and trivariate B-spline fitting using harmonic functions. *Computer Aided Geometric Design*, 26(6):648–664, 2009.
- [5] G. Xu, B. Mourrain, R. Duvigneau, and A. Galligo. Analysis-suitable volume parameterization of multi-block computational domain in isogeometric applications. *Computer-Aided Design*, 45(2):395 – 404, 2013.
- [6] X. Qian and O. Sigmund. Isogeometric shape optimization of photonic crystals via Coons patches. *Computer Methods in Applied Mechanics and Engineering*, 200:2237–2255, 2011.
- [7] T. W. Sederberg, J. Zheng, A. Bakenov, and A. Nasri. T-splines and T-NURCCs. In *ACM Transactions On Graphics (TOG)*, volume 22, pages 477–484. ACM, 2003.
- [8] Y. Bazilevs, V. M. Calo, J. A. Cottrell, J. A. Evans, T. J. R. Hughes, S. Lipton, M. A. Scott, and T. W. Sederberg. Isogeometric analysis using T-splines. *Computer Methods in Applied Mechanics and Engineering*, 199(5):229–263, 2010.
- [9] M. R. Dörfel, B. Jüttler, and B. Simeon. Adaptive isogeometric analysis by local h-refinement with T-splines. *Computer Methods in Applied Mechanics and Engineering*, 199(5):264–275, 2010.
- [10] M. A. Scott, X. Li, T. W. Sederberg, and T. J. R. Hughes. Local refinement of analysis-suitable T-splines. *Computer Methods in Applied Mechanics and Engineering*, 213:206–222, 2012.
- [11] Y. Zhang, W. Wang, and T. J. R. Hughes. Solid T-spline construction from boundary representations for genus-zero geometry. *Computer Methods in Applied Mechanics and Engineering*, 249:185–197, 2012.
- [12] W. Wang, Y. Zhang, L. Liu, and T. J. R. Hughes. Trivariate solid T-spline construction from boundary triangulations with arbitrary genus topology. *Computer-Aided Design*, 2012.
- [13] D. Burkhart, B. Hamann, and G. Umlauf. Isogeometric finite element analysis based on Catmull-Clark: subdivision solids. In *Computer Graphics Forum*, volume 29, pages 1575–1584. Wiley Online Library, 2010.
- [14] K. Li and X. Qian. Isogeometric analysis and shape optimization via boundary integral. *Computer-Aided Design*, 43(11):1427–1437, 2011.
- [15] M. A. Scott, R. N. Simpson, J. A. Evans, S. Lipton, S. P. A. Bordas, T. J. R. Hughes, and T. W. Sederberg. Isogeometric boundary element analysis using unstructured T-splines. *Computer Methods in Applied Mechanics and Engineering*, 254(0):197 – 221, 2013.
- [16] M.-J. Lai and P. Wenston. Bivariate splines for fluid flows. *Computers & Fluids*, 33(8):1047–1073, 2004.
- [17] G. Awanou and M.-J. Lai. Trivariate spline approximations of 3D Navier-Stokes equations. *Mathematics of Computation*, 74(250):585–602, 2005.
- [18] H. Speleers, C. Manni, F. Pelosi, and M. L. Sampoli. Isogeometric analysis with Powell-Sabin splines for advection-diffusion-reaction problems. *Computer Methods in Applied Mechanics and Engineering*, 2012.
- [19] H. Speleers, C. Manni, and F. Pelosi. From NURBS to NURPS geometries. *Computer Methods in Applied Mechanics and Engineering*, 255(0):238 – 254, 2013.
- [20] G. Farin. *Curves and surfaces for CAGD: A practical guide*. Morgan Kaufmann Publishers Inc., San Francisco, CA, USA, 5th edition, 2002.
- [21] M.-J. Lai and L. L. Schumaker. *Spline Functions on Triangulations*, volume 110. Cambridge University Press, 2007.
- [22] P. Alfeld and L. L. Schumaker. The dimension of bivariate spline spaces of smoothness for degree $d \geq 4r + 1$. *Constructive Approximation*, 3(1):189–197, 1987.
- [23] D. Hong. Spaces of bivariate spline functions over triangulation. *Approximation Theory and its Applications*, 7:56–75, 1991.
- [24] R. W. Clough and J. L. Tocher. Finite element stiffness matrices for analysis of plates in bending. In *Proceedings of the conference on Matrix Methods in Structural Mechanics*, 1965.
- [25] P. Percell. On cubic and quartic clough-tocher finite elements. *SIAM Journal on Numerical Analysis*, 13(1):100–103, 1976.
- [26] M. J. D. Powell and M. A. Sabin. Piecewise quadratic approximations on triangles. *ACM Transactions On Mathematical Software (TOMS)*, 3(4):316–325, 1977.
- [27] P. Dierckx. On calculating normalized Powell-Sabin B-splines. *Computer Aided Geometric Design*, 15(1):61–78, 1997.
- [28] E. Cohen, T. Lyche, and R. Riesenfeld. A B-spline-like basis for the Powell-Sabin 12-split based on simplex splines. *Mathematics of Computation*, 2013.
- [29] H. Speleers. A normalized basis for reduced Clough–Tocher splines. *Computer Aided Geometric Design*, 27(9):700–712, 2010.
- [30] H. Speleers. A normalized basis for quintic Powell–Sabin splines. *Computer Aided Geometric Design*, 27(6):438–457, 2010.
- [31] H. Speleers. Construction of normalized B-splines for a family of smooth spline spaces over Powell-Sabin triangulations. *Constructive Approximation*, 37(1):41–72, 2013.
- [32] M.-C. Rivara. New mathematical tools and techniques for the refinement and or improvement of unstructured triangulations. In *5th International Meshing Roundtable*, pages 77–86, 1996.
- [33] P. Alfeld. Bivariate spline spaces and minimal determining sets. *Journal of Computational and Applied Mathematics*, 119(1):13–27, 2000.
- [34] H. Prautzsch, W. Boehm, and M. Paluszny. *Bezier and B-spline techniques*. Springer-Verlag New York, Inc., Secaucus, NJ, USA, 2002.
- [35] J. Fish and T. Belytschko. *A first course in finite elements*. John Wiley and Sons, Ltd, 2007.
- [36] T. J. R. Hughes. *The Finite Element Method: Linear static and dynamic finite element analysis*. Dover Publications, 2000.
- [37] P. L. Gould. *Introduction to linear elasticity*. Springer-Verlag, 1999.